HAL
open science

Exciton band structure of Molybdenum Disulfide: from monolayer to bulk

Giorgia Fugallo, Pierluigi Cudazzo, Matteo Gatti, Francesco Sottile

To cite this version:

Giorgia Fugallo, Pierluigi Cudazzo, Matteo Gatti, Francesco Sottile. Exciton band structure of Molybdenum Disulfide: from monolayer to bulk. Electronic Structure, 2021, 3 (1), pp.014005. 10.1088/2516-1075/abdb3c . hal-03190274

HAL Id: hal-03190274

https://hal.science/hal-03190274

Submitted on 6 Apr 2021

HAL is a multi-disciplinary open access archive for the deposit and dissemination of scientific research documents, whether they are published or not. The documents may come from teaching and research institutions in France or abroad, or from public or private research centers.

L'archive ouverte pluridisciplinaire **HAL**, est destinée au dépôt et à la diffusion de documents scientifiques de niveau recherche, publiés ou non, émanant des établissements d'enseignement et de recherche français ou étrangers, des laboratoires publics ou privés.

Exciton band structure of Molybdenum Disulfide: from monolayer to bulk

Giorgia Fugallo,[1,2,*] Pierluigi Cudazzo,[3,4,2] Matteo Gatti,[3,5,2] and Francesco Sottile[3,2]

[1] *Laboratoire de Thermique et Energie de Nantes, UMR 6607 CNRS PolytechNantes, Université de Nantes, 44306 Nantes, France*

[2] *European Theoretical Spectroscopy Facility (ETSF)*

[3] *Laboratoire des Solides Irradiés, École Polytechnique, CNRS, CEA/DRF/IRAMIS, Institut Polytechnique de Paris, F-91128 Palaiseau, France.*

[4] *Physics and Materials Science Research Unit, University of Luxembourg, 162a Avenue de la Faïencerie, L-1511 Luxembourg, Luxembourg*

[5] *Synchrotron SOLEIL, L'Orme des Merisiers, Saint-Aubin, BP 48, F-91192 Gif-sur-Yvette, France*

Exciton band structures analysis provides a powerful tool to identify the exciton character of materials, from bulk to isolated systems, and goes beyond the mere analysis of the optical spectra. In this work, we focus on the exciton properties of Molibdenum Disulfide (MoS_2) by solving the ab initio many-body Bethe-Salpeter equation, as a function of momentum, to obtain the excitation spectra of both monolayer and bulk MoS_2. We analyse the spectrum and the exciton dispersion on the basis of a model excitonic Hamiltonian capable of providing an efficient description of the excitations in the bulk crystal, starting from the knowledge of the excitons of a single layer. In this way, we obtain a general characterization of both bright and darks excitons in terms of the interplay between the electronic band dispersion (i.e. interlayer hopping) and the electron-hole exchange interaction. We identify for both the 2D and the 3D limiting cases the character of the lowest-energy excitons in MoS2, we explain the effects and relative weights of both band dispersion and electron-hole exchange interaction and finally we interpret the differences observed when changing the dimensionality of the system.

I. INTRODUCTION

Layered materials and their two-dimensional (2D) building blocks have remarkable properties that give them a high potential of technological relevance. Boosted by the first isolation of graphene in 2005[1], the number of studies on these materials has been growing in the last decades at a rather fast pace[2–7]. The impressive attention devoted to their uncommon structural, thermal and optical properties motivates the pursuit of a clear understanding of all the physical processes responsible for their properties that could ultimately allow to tailor new materials (e.g. Van der Waals heterostructures) with desired properties[6,7].

Among the successors of graphene, transition metal dichalcogenides (TMDs) are subject of intense study both on the experimental and the theoretical side for a number of reasons, among which: i) contrary to graphite/graphene, TMDs show a finite band gap, which, in view of their recent availability in the form of high-quality single layer flakes[8], makes them natural candidates for opto-electronic applications; ii) like all layered materials, they present fascinating features in the transition from the 3D to their 2D building blocks, mainly due to the effects of van der Waals (vDW) forces; in particular, their electronic band gap goes from being indirect (3D) to direct (2D); iii) the coupling between real spin and valley pseudo-spin[9], due to a break of the inversion symmetry in their structure, can give rise to valley dependent optical selection rules[10–14]; iv) TMD are perfectly suited as the active material in cavity quantum electrodynamics. This is thanks to the giant oscillator strength of their excitons that give rise to well-pronounced optical transitions which can be brought into resonance with electromagnetic fields in plasmonic nanostructures and microcavities[15–18]; v) in monolayer TMDs, electron-hole (e-h) interactions are much stronger than in conventional semiconductors, due to the reduced effective screening[19,20] and carrier confinement in a single atomic layer - common features of all the 2D systems- in combination with large carrier effective masses (see Ref. 21 and references therein); that leads to the impossibility to use the standard hydrogenic model in 2D limit and makes meaningless the usual classification of strong and weak exciton based on the binding energy. On the contrary, the investigation of the exciton dispersion as a function of momentum $\mathbf{q}$, which can be experimentally accessed by electron energy loss spectroscopy[22], is capable to reveal the exciton character also in 2D[23]. Finite-momentum excitons are dark since they cannot be optically excited[24]. However, dark excitons play a key role for many disexcitation processes, like for example phonon-assisted luminescence and light emission. Moreover, thanks to recent experimental advances[25,26] it has been shown that dark excitons can be experimentally probed by applying an in-plane magnetic field. This important results shows another reason for using a theoretical and computational technique, able to follow and explain the dispersion of both bright and dark excitations, well understanding their character and the interplay between the two.

In the last years, the theoretical community has started putting an effort on the numerical evaluation of the exciton dispersion, mainly around the regions close the band extrema, of monolayer TMDs. Already in this reduced small subspace there are many interesting phenomena,

but a complete picture is becoming more and more necessary, for all the reasons mentioned above as well as for modelling how excitons in TMDCs couple to localized electric fields and explaining , among other phenomena, also localized plasmon-exciton coupling[27]. In this respect MoS_2, with its remarkable versatile excitonic landscape, can be considered a perfect prototypical material of the wide class of TMDs[23,24,28–33]. At the same time there has been a growing interest in finding models able to give simple physical insights on the interplay between electron-hole exchange interaction and band dispersion in the transition between the 3D and the 2D limit cases[30,34–36].

In this paper we study, within an *ab initio* framework, exciton band structure of MoS_2 with the help of a model that describes excitons in layered crystals starting from the knowledge of the excitons in a single layer. Our model, on top of the solution of the Bethe-Salpeter equation[37,38], the state-of-the-art method to describe excitonic effects in condensed matter, has been already successfully used for hexagonal boron nitride hBN[36]. We here show that it allows one to distinguish excitons of different character in a simple manner and to well describe at the same time materials with a predominance of Frenkel excitons, such as hBN, and materials with a predominance of Wannier ones, such as MoS_2.

Provided with this tool, we carry out an analysis of the exciton dispersion of MoS2, as we go from the monolayer 2D system to 3D bulk, and perform a comparison between the two limiting cases. We perform our study not only around the electronic bands extrema, but all along both ΓM and ΓK high symmetry lines, for analysing the link between the exciton dispersions and the intrinsic anistropy of the structure. We show how the exciton dispersion is strongly affected by the electronic band structure, due to the predominance of the Wannier character, and how this feature affects the 2D and the 3D case differently.

II. THEORETICAL FRAMEWORK AND COMPUTATIONAL DETAILS

The BSE is a formally exact Dyson-like equation for the polarizability of a system. In the standard approach[39,40], it can be cast into an effective two-particle Schrödinger equation for the wavefunction $\Psi^{\lambda}_{\mathbf{q}}(\mathbf{r}_h, \mathbf{r}_e)$ of the electron-hole (e-h) pair: $H_{\rm exc}\Psi^{\lambda} = E^{\lambda}\Psi^{\lambda}$. Within the GW approximation[41] to the BSE[37–39], the excitonic Hamiltonian $H_{\rm exc} = H_{\rm e} + H_{\rm h} + H_{\rm e-h}$ is the sum of the independent propagations (i.e. hoppings) $H_{\rm e}$ and $H_{\rm h}$ of the electron and the hole (which derive from the GW quasiparticle (QP) band structure) and the e-h interaction $H_{\rm e-h}$, which includes the exchange electron-hole repulsion due to the bare Coulomb interaction $\bar{v}_c$ (the modified Coulomb interaction $\bar{v}_c$ is defined such that its long-range term, i.e. its G=0 component in reciprocal space, is set to zero[39], and the direct electron-hole attraction due to the statically screened Coulomb interaction W. The solution of the BSE is used to construct the macroscopic dielectric function $\epsilon_M(\mathbf{q},\omega)$, from which spectra are obtained.

In Ref.36 we have rewritten $H_{\rm exc}$ in the basis of wavefuctions localized on the elementary units of the layered system, namely the single layers. This simplified model works under the assumption that: i) the one-particle wavefuctions, localized on different layers, do not overlap; ii) they can be factorized in an in-plane and out-of-plane components; iii) different layers stacked along z-axis can be rotated one with respect to another; iv) for each layer a two-band system is considered. Under this simplified model the whole excitonic Hamiltonian takes then the simple form of the sum of three terms $\hat{H}_{exc} = \hat{H}_{ip} + \hat{K}_{CT} + \hat{K}_{FR}$ which can be written[36]:

$$\begin{aligned}
\hat{H}_{ip} &= \sum_{\mathbf{k}_1\mathbf{k}_2}\sum_{\mathbf{RS}}\sum_{ij} E_c^{\mathbf{R}i\mathbf{S}j}(\mathbf{k}_1,\mathbf{k}_2) a^{\dagger}_{c\mathbf{k}_1\mathbf{R}i} a_{c\mathbf{k}_2\mathbf{S}j} - \sum_{\mathbf{k}_1\mathbf{k}_2}\sum_{\mathbf{RS}}\sum_{ij} E_v^{\mathbf{R}i\mathbf{S}j}(\mathbf{k}_1,\mathbf{k}_2) b^{\dagger}_{v\mathbf{k}_1\mathbf{R}i} b_{v\mathbf{k}_2\mathbf{S}j} \\
\hat{K}_{FR} &= \sum_{\mathbf{k}_1\mathbf{k}_2\mathbf{k}_3\mathbf{k}_4}\sum_{\mathbf{R}i,\mathbf{S}j}\left[\bar{v}^{\mathbf{S}j,\mathbf{S}j}_{\mathbf{R}i,\mathbf{R}i}(v\mathbf{k}_1c\mathbf{k}_2v\mathbf{k}_3c\mathbf{k}_4) - \delta_{\mathbf{R}i,\mathbf{S}j} W^{\mathbf{R}i,\mathbf{R}i}_{\mathbf{R}i,\mathbf{R}i}(v\mathbf{k}_1c\mathbf{k}_2v\mathbf{k}_3c\mathbf{k}_4)\right] a^{\dagger}_{c\mathbf{k}_2\mathbf{R}i} b^{\dagger}_{v\mathbf{k}_1\mathbf{R}i} b_{v\mathbf{k}_3\mathbf{S}j} a_{c\mathbf{k}_4\mathbf{S}j} \\
\hat{K}_{CT} &= -\sum_{\mathbf{k}_1\mathbf{k}_2\mathbf{k}_3\mathbf{k}_4}\sum_{\mathbf{R}i,\mathbf{S}j}(1-\delta_{\mathbf{R}i,\mathbf{S}j}) W^{\mathbf{S}j,\mathbf{R}i}_{\mathbf{S}j,\mathbf{R}i}(v\mathbf{k}_1c\mathbf{k}_2v\mathbf{k}_3c\mathbf{k}_4) a^{\dagger}_{c\mathbf{k}_2\mathbf{R}i} b^{\dagger}_{v\mathbf{k}_1\mathbf{S}j} b_{v\mathbf{k}_3\mathbf{S}j} a_{c\mathbf{k}_4\mathbf{R}i},
\end{aligned} \tag{1}$$

in which $\mathbf{k} \in$ 1BZ, and v(c) denote a valence (conduction) Bloch state of energy $E_v(E_c)$ calculated within the GWA; $a^{\dagger}$ (a) and $b\dagger$ (b) are the creation (annihilation) operators for electrons and holes, $\mathbf{R}, \mathbf{S}$ are the lattice vectors along z and the index i denotes the layers inside the unit cell. $\hat{H}_{ip}$ describes then the scattering process from layer to layer, independently for electrons and holes, with

$$E^{\mathbf{R}i\mathbf{S}j}_{v(c)}(\mathbf{k}_1,\mathbf{k}_2) = E^{i}_{v(c)}(\mathbf{k}_1)\delta_{\mathbf{R}i,\mathbf{S}j}\delta_{\mathbf{k}_1,\mathbf{k}_2} + t^{v(c)\mathbf{k}_1,\mathbf{k}_2}_{\mathbf{R}i,\mathbf{S}j}, \tag{2}$$

with then $E^{i}_{v(c)}(\mathbf{k}_1)$ is the single-layer band dispersion and $t^{v(c)\mathbf{k}_1,\mathbf{k}_2}_{\mathbf{R}i,\mathbf{S}j}$ are interlayer hopping matrix elements that give rise to the finite k_z dispersion of the bands in the crystal. $\hat{K}_{\rm FR}$ and $\hat{K}_{\rm CT}$ describe the interaction between

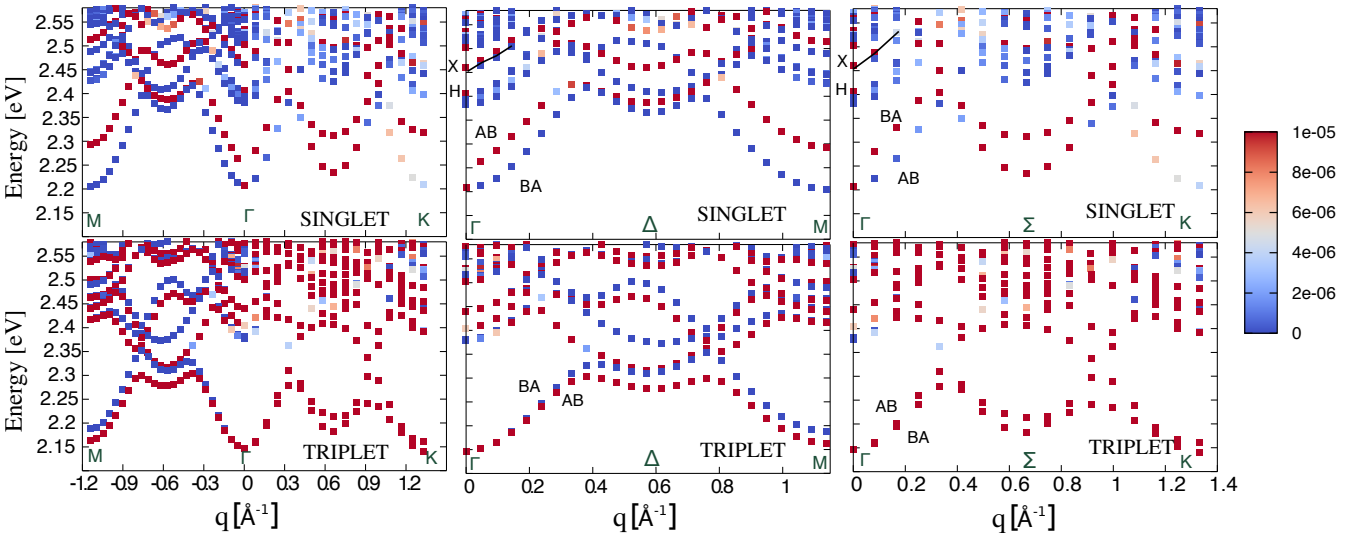

FIG. 1. Exciton band structure in monolayer MoS_2 for in-plane $\mathbf{q}$ along (left panels) MΓK , (central panels) ΓM and (right panels) ΓK hight symmetry lines in the first Brillouin Zone. Both (top panels) Singlet and (bottom panels) triplet excitons are reported for comparison. The two lowest excitons AB and BA are inverted by symmetry[34,35] moving along ΓM and ΓK

an electron and a hole that are localized on the same layer or on different layers, respectively. The subscripts FR and CT are used to remind one about Frenkel and Charge Transfer concepts, a terminology that is common for other van der Waals materials like molecular solids[42]. However, in the present context a FR state is an intralayer exciton that is fully localised on a single layer, independently on its (de)localisation within the layer, whereas a CT state is an interlayer exciton. Therefore this definition, already applied for hBN[36] where the exciton is tightly bound within the single layer[43] , can be also applied here for MoS_2, or other layered materials, where it is more weakly bound[44]. The FR and CT interaction terms are coupled by the interlayer hopping terms in $\hat{H}_{ip}$. Without these terms $t^{v(c)\mathbf{k}}_{\mathbf{R}i,\mathbf{S}j}$ the excitonic hamiltonian in Eq. (1) factorizes into two independent blocks: a CT hamiltonian $\hat{H}_{CT} = \hat{H}'_{ip} + \hat{K}_{CT}$ describing an interacting e-h pair localised on different layers and a FR hamiltonian $\hat{H}_{FR} = \hat{H}'_{ip} + \hat{K}_{FR}$ describing an interacting e-h pair on the same layer (in both cases we set $t^{v(c)\mathbf{k}}_{\mathbf{R}i,\mathbf{S}j} = 0$ in H'_{ip}). This form for the $\hat{H}_{\rm exc}$ illustrates much more clearly the physics of excitons in layered materials. In fact in this reformulation a FR exciton can be seen, in analogy with molecular crystals, as an elementary excitation of a single layer, which can scatter from one layer to another due to the interlayer coupling[36].

In our first-principles calculations we obtain the single-particle states using Kohn-Sham (KS) density-functional theory within the local-density approximation (LDA)[45]. We use Troullier-Martins pseudopotentials[46], and expand the KS wavefunctions in a plane-wave basis set with a cutoff of 20 (50) Hartree for the bulk (the monolayer). The lattice parameters for the bulk were taken equal to the experimental values[47] while for the monolayer (in order to ensure the direct band gap) it has been taken from Ref. 44. The main feature of the single layer MoS_2 electronic band structure is indeed the direct fundamental

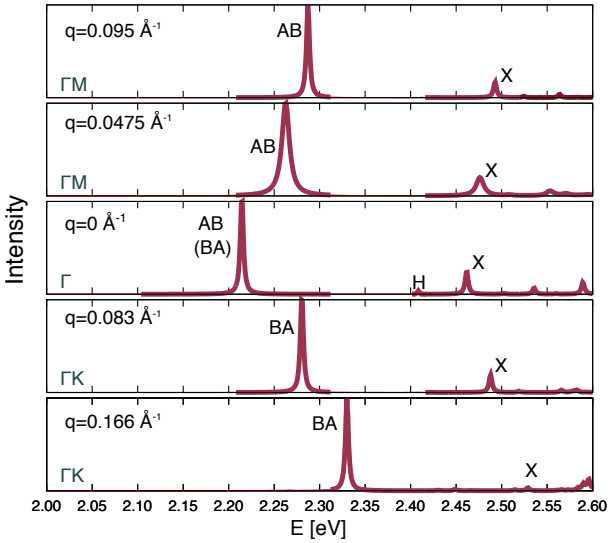

FIG. 2. Im$\epsilon(\mathbf{q},\omega)$ around Γ-point (center panel) in comparison with the first two $\mathbf{q}$ point along ΓM towards up and ΓK towards down. All the peaks presented in the graph are within the smallest independent -particle GW transition energy.

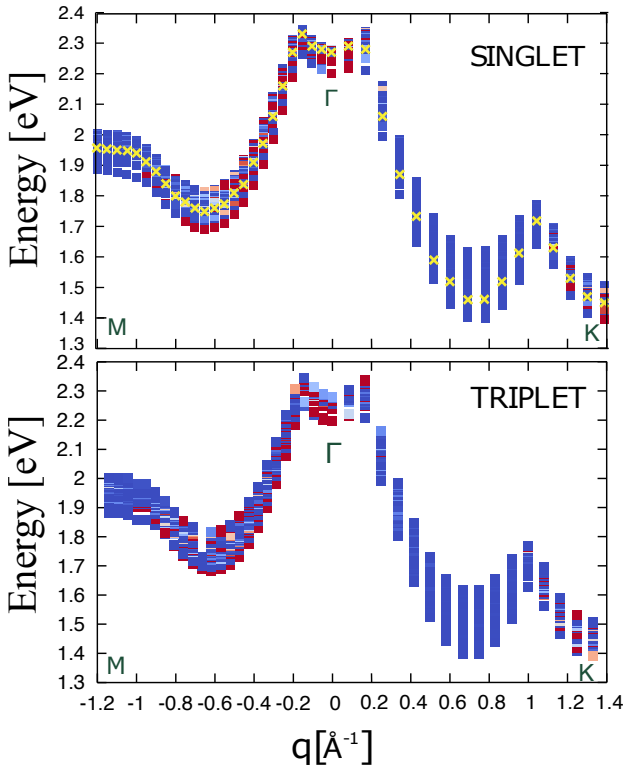

FIG. 3. Exciton band structure in bulk MoS2 for in-plane **q** along MΓK high symmetry lines. Both (top panel) singlet and (bottom panel)triplet excitons are reported for comparison. Yellow crosses indicate the dispersion of the smallest independent particle GW-transition energies associated to each **q**

band gap, even though it crucially depends on the lattice geometry and even small differences can induce significant changes[21]. Other important features in the band structure of monolayer and bulk MoS_2 are due to spin orbit coupling (SOC). In the monolayer, the SOC splits the valence band maximum at the K point of $\sim$ 150 meV[44,48–50]. This splitting explains the doublet structure of the strong peak in the absorption spectrum and it is conventionally used to classify the peaks into A and B series[51]. The conduction band minimum, also located at the K point, is less affected by the SOC and the splitting is one order of magnitude smaller than for the valence bands. In the bulk, the SOC has only the effect of increasing of 80 meV[50] the splitting already present of 160 meV in the two top valence bands at the K point due to the interlayer interactions. In our calculations we will not consider the SOC for simplicity. So instead of the A and B series in monolayer we will label the exciton as AB.

We simulate the results of GW calculations for MoS_2 bulk (monolayer)[44,49], by applying a scissor operator of 0.56 eV (0.98 eV) to correct for the LDA underestimation of the single-particle band gap. For the BSE calculations, which are run on top of the GW band-structure, we sample the Brillouin zone of the bulk (monolayer) using a 48×48×4 (48×48×1) Γ-centered k-grid . To simplify the analysis of the results we use a minimal e-h transition basis set including 2 valence and 2 conduction bands and solve the BSE within Tamm-Dancoff Approximation (TDA)[52,53]. Coupling between resonant and antiresonant transitions beyond the TDA has been found numerically negligible[32]. In the construction of the BSE hamiltonian, we expand the single-particle states and static dielectric function with plane-wave cutoffs up to 344 and 131 eV, respectively. We have adopted a supercell approach, using a truncation of the Coulomb interaction $\bar{v}_c$[54,55] to prevent interactions between periodic copies. Moreover, we have avoided divergences of Coulomb integrals by means of a 2D analytical integration that efficiently removes the Coulomb singularity[23]. We perform the KS and static screening calculations using ABINIT[56], and BSE calculations with EXC[57]. All the spectra presented in the following sections are calculated for in-plane momentum transfer **q** along both the ΓM and ΓK directions.

III. RESULTS

IV. MONOLAYER

In Fig. 1 we report the 40 lowest eigenvalues of the excitonic hamiltonian $H_{\rm exc}$ as a function of **q** for the singlet and triplet states, where for the latter the e-h exchange interaction has been switched off. The colour scale represents their intensity. Red squares are for states that have a visible peak in $\mathrm{Im}\epsilon_{\rm M}(\mathbf{q},\omega)$, while blue squares are dark exciton states with no intensity in the spectrum. With respect to the singlet excitons, the triplet energies are globally lower as the e-h exchange interaction is repulsive and hence yields singlet states to have higher energies than the corresponding triplets.

As already pointed out[29,58,59] the hydrogenic model deviates from the ab initio results in two significant ways: i) the binding energies of excited states are much larger than expected from a 2D hydrogenic model; and ii) states with higher angular momentum have a larger binding energy than states with lower angular momentum.[30]. Both for A and B excitons (in our case the single AB), the valley states degenerate at the Brillouin-zone center (Γ-point), due to the time-reversal symmetry, split at small momentum into a lower dark mode with quadratic dispersion and an upper bright mode with linear dispersion[28,29,44,58,59]. This unusual pattern is due the $1/q$ behaviour of the Coulomb interaction in 2D[28,29,60]. This is confirmed by the fact that exciton energies for triplet states with no exchange e-h interaction remain almost doubly degenerate also at finite **q** as shown in the lower panels of Fig. 1. The tiny separation is due to **q** dependence of the matrix elements of the direct e-h attraction W[60]. The effect of the e-h exchange is

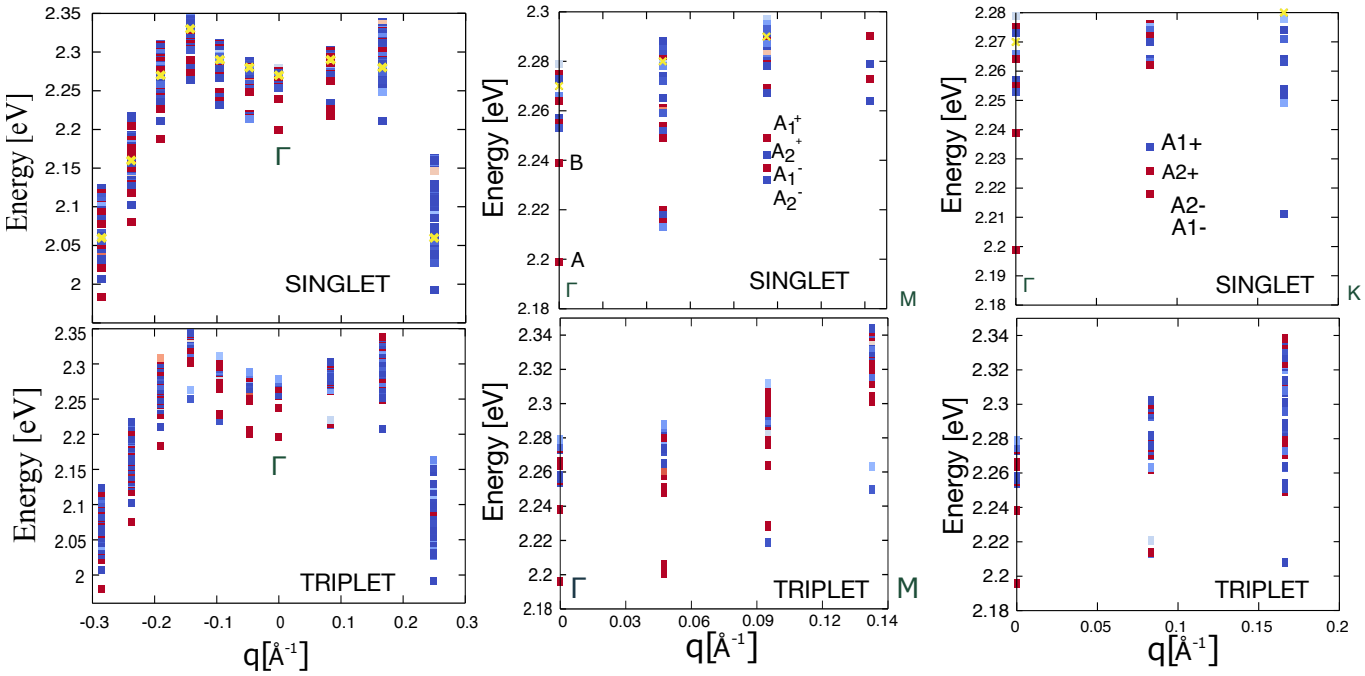

FIG. 4. Zoom of the exciton band structure in bulk MoS2 for in-plane $\mathbf{q}$ around Γ (left panels), and for the first $\mathbf{q}$ points along ΓM (central panels) and ΓK (right panels) Both (top panels) singlet and (bottom panels) triplet excitons are reported for comparison. Yellow crosses indicate the dispersion of the smallest independent particle GW-transition energies associated to each $\mathbf{q}$

evident also at Brillouin zone borders, where the separation between the lower bands is bigger for singlet states than for the triplet ones.

The in-plane MoS_2 anisotropy[21,61] can be easily inferred from Fig. 1 where the exciton response changes if moving along the in-plane high symmetry line ΓM or ΓK. Nevertheless there is a small region around Γ (for $\mathbf{q}$ up to 0.3 $Å^{-1}$) where the exciton band dispersion is almost perfectly symmetric. This feature is well visible also in Fig.2, where $\mathrm{Im}\epsilon_{\mathrm{M}}(\mathbf{q},\omega)$ of the monolayer MoS_2 is displayed at Γ (central panel) and for two smallest $\mathbf{q}$ along both Γ-M (upper panels) and ΓK (lower panels). At $\mathbf{q} = 0$ the prominent peak AB at 2.206 eV is the tightly bound exciton associated with the so-called A (B)-series in literature (when in presence of SOC), with a binding energy of 0.61 eV in agreement with Ref.29 and 62. This exciton is degenerate with a dark state BA. AB and BA are inverted for symmetry reasons[34,35] if moving along ΓM or ΓK, so that the bright exciton will be AB or BA moving respectively along ΓM or along ΓK. We can also see for $\mathbf{q} = 0$ the presence of other peaks, namely H at 2.406 eV and X at 2.46 eV. These peaks are both: i) still inside the gap (which in GW amount to 2.7 eV) , ii) doubly degenerate and iii) due to direct transitions between top valence band and lowest bottom conduction in the valley K (K'). At finite $\mathbf{q}$ the degeneracy is removed by the e-h exchange coupling such as for the AB peak but while X splits in one bright and one dark state (see Fig.1) with respectively a linear and a quadratic dispersion, H splits in two dark states and disappears at finite $\mathbf{q}$ in both direction ΓM and ΓK as easily observable in Fig.1. Low-energy exciton states appear both near the Brillouin-zone center and near the Brillouin-zone corners. There are two distinct types of Brillouin-zone corner excitons. Specifically looking at Fig. 1 (left and right panels), the first four excitons at $\mathbf{q}$ =K are respectively due to transition K-K' for the first (bright) and third (dark) exciton and Γ-K for the second (bright) exciton, while the forth exciton has an hybrid character being built on transitions K-K' and Γ-K. The possibility to have for $\mathbf{k}$ =K both transitions K-K' and ΓK is associated to the hexagonal BZ[63]. In fact by adding a momentum $\mathbf{q}$ = ΓK to $\mathbf{k}$ =K one obtains another $\mathbf{k}' = \mathbf{k} + \mathbf{q}$ =K . Low-energy exciton states appear also at the side-center M of the BZ ((left and central panels of Fig. 1 . These states are due to ΓM transitions. It is interesting to notice that the in-plane anisotropy starts to become visible when, moving along ΓK or ΓM, one starts approaching the high symmetry points Σ or Δ. Looking at the electronic band structure (see Fig.6) it is easy to observe that the lowest conduction band shows a local minimum both at Σ and Δ. Nevertheless the band dispersion is different around these points, as well as the energy of the minimum. This difference in the electronic band structure is directly reflected also in the exciton dispersion. Mimicking the electronic band dispersion, the exciton dispersion shows two local

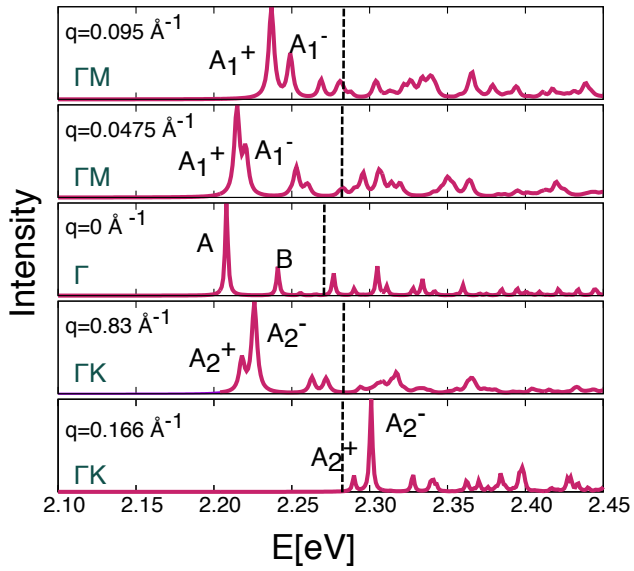

FIG. 5. Im$\epsilon(\mathbf{q},\omega)$ around Γ-point (center panel) in comparison with the first two $\mathbf{q}$ point along ΓM towards up and ΓK towards down. The dashed vertical lines mark the smallest independent-particle GW transition energy. It should be noted that the number of bands included in these calculations only ensure the convergency up to the position of the A and B excitons, not much above.

minima at Σ and Δ but the minimum in Σ is much more pronounced than that one in Δ. Moreover even if the effect of the e-h exchange is numerically equivalent along ΓK and ΓM, in the latter case it leads to a swap between the bright (AB) and the dark (BA) exciton.

A. Bulk

In Fig. 3 the 40 lowest eigenvalues of the MoS_2 bulk excitonic hamiltonian are shown. Once again the dispersion is strictly connected to the electronic band structure (Fig.6). The general shape follows closely the dispersion of the smallest independent particle GW-transition energies associated to each $\mathbf{q}$ (reported as yellow crosses on Fig.3). With respect to the monolayer case, bulk MoS_2 shows a more pronounced in plane anisotropy. In the bulk the local minimum in the lowest conduction band at Σ is much lower than at Δ. Moreover its energy is very close to the energy of the absolute minimum in K. This different feature of the electronic band structures leads to an en equivalent anisotropy in the exciton dispersion.

Looking at the spectra around Γ (compare Fig. 2 and Fig. 5) monolayer and bulk presents a similar line-shape: one prominent peak AB in monolayer and two in bulk (even without the SOC the two top valence bands are split), followed by minor peaks. The main differences arise from the exciton binding energy which decreases with the number of layers. While all the peaks shown in Fig.2 for the monolayer case were inside the gap, only the first two peaks A and B in bulk are bound excitons. These peaks are the collective contribution of several excitons due to parallel transitions at K. The reason of this decrease in the binding energy is related, as already mentioned, to a larger dielectric screening in bulk. Moreover while the high-energy excitons exhibit sharp peaks in the monolayer, they are difficult to be distinguished one another in the bulk. Experimental observation confirms a broader adsorption for bulk MoS_2 in contrast to relatively narrow peaks in monolayer MoS_2[64–66]. The intensity of the excitonic peaks is directly related to the spatial localization of the exciton correlation function. As others have shown (see Ref. 21 and references therein), exciton correlation function both in monolayer and bulk mainly lies on Mo atoms with only a tiny fraction outside the layer. Therefore the excitons (A and B) remain in one layer, without coupling between layers, and optical transitions take place within the same layer. This feature, already observed also in hBN[67], confirms once more the validity of our model[36].

We can see that, in analogy of what found for hBN, for each of the two lowest degenerate excitons AB and BA present in the monolayer one has four excitons in bulk.

This happens because if we consider a crystal with two inequivalent layers per unit cell, as is the case of MoS2, for each quantum number λ that defines an excitation of the single layer one has four excitons in the bulk. The FR and CT excitons that diagonalize the excitonic Hamiltonian in Eq.(1) in the absence of interlayer hopping are then the symmetric and antisymmetric combinations with respect to the exchange of the e-h pair between two inequivalent layers. So, in the present case, out of 8 excitons, 4 are FR and 4 are CT excitons. In an ideal case of no interlayer hopping, we would expect that the two lowest AB and BA excitons of MoS_2 single layer give rise in the bulk to 3 dark plus 1 visible FR exciton, together with CT excitons at higher energies. In the real case, the hopping is always present and its effect is to couple FR and CT excitons. This coupling produces states with mixed character, FR+CT and CT+FR respectively, and modifies their energies.

In hBN[36] at $\mathbf{q} = 0$ excitons with different parities do not couple, giving rise to states with well defined parity, with a finite Davydov splitting between symmetric and antisymmetric excitons induced by the hopping. Only at finite $\mathbf{q}$, the different excitons formally lose their parity character and are allowed to mix together.

In MoS_2, on the opposite, at $\mathbf{q} = 0$ the four lowest singlet and triplet excitons are all degenerate. This different behaviour in MoS_2 is due to the differences in the out of plane electronic band dispersion (see Fig. 6). The k_z dispersion of the top valence and bottom-conduction single-particle band is almost negligible, this is equivalent to say that the inter-layer hopping is reduced so much to not yield any Davydov splitting between symmetric and

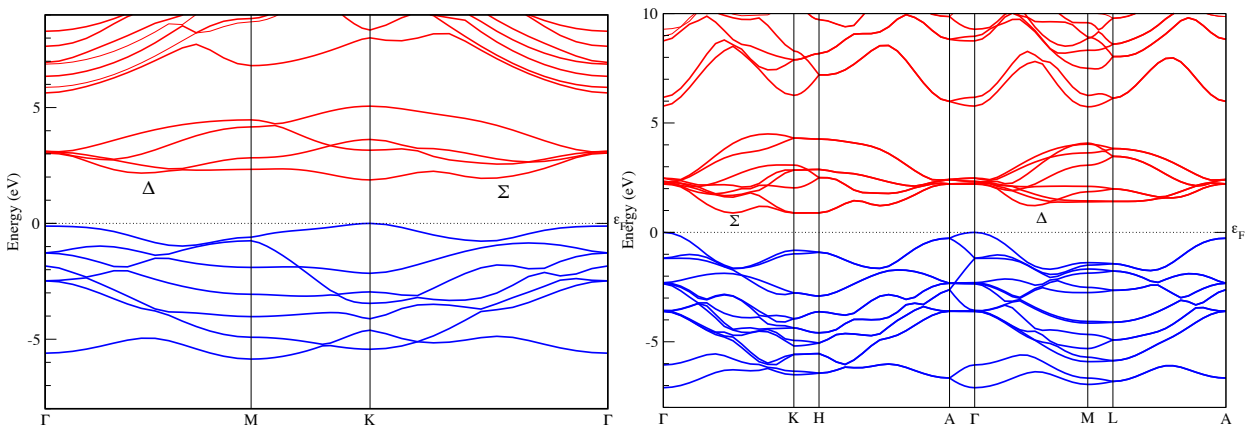

FIG. 6. QP band structure of mono (left panel) and bulk (right panel) MoS_2.

antisymmetric excitons at $\mathbf{q} = 0$ (like in the molecular crystal case[42].)

Both the first 4 degenerate excitons and the second 4 degenerate ones are due to direct transitions at the valleys K or K'.

In analogy to hBN then, at finite $\mathbf{q}$ the interlayer hopping mixes FR and CT states with different parities $|(FR+CT)^{\lambda}_{\pm}|$, such that the dark exciton $|(FR+CT)^{A_1^-}|$ ($|(FR+CT)^{A_2^-}|$) along ΓM (ΓK)is switched on by the effective coupling with the visible exciton $|(FR+CT)^{A_1^+}|$ ($|(FR+CT)^{A2^+}|$). In Fig. 5 we labelled the first 4 exciton with A_1^-,A_1^+,A_2^-, A_2^+ . Moving along ΓM (ΓK) the visible excitons will be A_1^-, A_1^+ (A_2^-, A_2^+) . The same discussion can be carried on for the higher energy exciton B. Taking a look at Fig. 4 and Fig. 5 , it is possible to see immediately another effect of the larger in plane-anisotropy in bulk. Already for a momentum transferred $\mathbf{q} = -0.166\text{Å}^{-1}$ along ΓK the $A_2^{\pm}$ visible states are lost in the continuous, while the lower energies dark excitons are due to transitions along ΓΣ . The exciton dispersion also in this case reflects the shape of the electronic band structure.

V. SUMMARY

By the solution of the ab initio Bethe-Salpeter equation (BSE) as a function of momentum $\mathbf{q}$, we have obtained the eigenvalue spectrum of the excitonic Hamiltonian for the electronic excitations of MoS_2. We have then discussed and explained the properties of both visible and dark excitons on the basis of a simplified model for layered system[36] which shows explicitly the interplay between the electronic band dispersion and the electron-hole exchange interaction. By extending such a model to MoS_2 we have proven its strength in analysing not only material with predominance of Frenkel excitons but also, as in the present case, of Wannier one. We have shown the influence of the electronic structure in the full exciton dispersion in the BZ and the much stronger impact of anisotropy in bulk with respect to the monolayer case. In the monolayer, in-plane anisotropy starts to become visible when one starts approaching the high symmetry points Σ or Δ where the electronic bands show local minima but at slightly different energies and with different dispersions. In the bulk, where the differences in the electronic band structure around Σ and Δ are larger, we witness to an enhanced anysotropy in the exciton band structure, which is detectable much closer to Γ than in the corresponding 2D case. The predominant Wannier character is translated into an exciton dispersion that, even though it reflects the electronic band structure, it exihibits an amplifying effect: small differences in the electronic structure will be more pronounced in the exciton collective response.

Acknowledgments

This work was performed using HPC resources from GENCI- [TGCC/CINES/IDRIS] within Projects No. 100834 and 0544.

* giorgia.fugallo@univ-nantes.fr

[1] K. S. Novoselov, D. Jiang, F. Schedin, T. J. Booth, V. V.

Khotkevich, S. V. Morozov, and A. K. Geim, Proceedings of the National Academy of Sciences of the United States of America **102**, 10451 (2005).
[2] M. S. Dresselhaus, G. Dresselhaus, and P. C. Eklund, *Science of Fullerenes and Carbon Nanotubes: Their Properties and Applications* (Academic Press, 1996).
[3] M. Dresselhaus, R. Smalley, G. Dresselhaus, and P. Avouris, *Carbon Nanotubes: Synthesis, Structure, Properties, and Applications*, Topics in Applied Physics (Springer Berlin Heidelberg, 2003).
[4] V. I. Klimov, ed., *Semiconductor and Metal Nanocrystals: Synthesis and Electronic and Optical Properties* (CRC Press, 2003).
[5] P. Moriarty, Reports on Progress in Physics **64**, 297 (2001).
[6] A. K. Geim and I. V. Grigorieva, Nature **499**, 419 (2013).
[7] K. S. Novoselov, A. Mishchenko, A. Carvalho, and A. H. Castro Neto, Science **353** (2016), 10.1126/science.aac9439.
[8] J. N. Coleman, M. Lotya, A. O'Neill, S. D. Bergin, P. J. King, U. Khan, K. Young, A. Gaucher, S. De, R. J. Smith, I. V. Shvets, S. K. Arora, G. Stanton, H.-Y. Kim, K. Lee, G. T. Kim, G. S. Duesberg, T. Hallam, J. J. Boland, J. J. Wang, J. F. Donegan, J. C. Grunlan, G. Moriarty, A. Shmeliov, R. J. Nicholls, J. M. Perkins, E. M. Grieveson, K. Theuwissen, D. W. McComb, P. D. Nellist, and V. Nicolosi, **331**, 568 (2011).
[9] D. Xiao, G.-B. Liu, W. Feng, X. Xu, and W. Yao, Phys. Rev. Lett. **108**, 196802 (2012).
[10] T. Cao, G. Wang, W. Han, H. Ye, C. Zhu, J. Shi, Q. Niu, P. Tan, E. Wang, B. Liu, and J. Feng, Nature Communications **3**, 887 EP (2012), article.
[11] H. Zeng, J. Dai, W. Yao, D. Xiao, and X. Cui, Nat Nano **7**, 490 (2012).
[12] K. F. Mak, K. He, J. Shan, and T. F. Heinz, Nat Nano **7**, 494 (2012).
[13] T. Yu and M. W. Wu, Phys. Rev. B **93**, 045414 (2016).
[14] H. Bragança, F. Riche, F. Qu, V. Lopez-Richard, and G. E. Marques, Scientific Reports **9**, 4575 (2019).
[15] C. Schneider, M. M. Glazov, T. Korn, S. Höfling, and B. Urbaszek, Nature Communications **9**, 2695 (2018).
[16] H. Li, M. Qin, Y. Ren, and J. Hu, Opt. Express **27**, 22951 (2019).
[17] H. Li, B. Chen, M. Qin, and L. Wang, Opt. Express **28**, 205 (2020).
[18] C. Janisch, H. Song, C. Zhou, Z. Lin, A. L. Elías, D. Ji, M. Terrones, Q. Gan, and Z. Liu, 2D Materials **3**, 025017 (2016).
[19] P. Cudazzo, I. V. Tokatly, and A. Rubio, Phys. Rev. B **84**, 085406 (2011).
[20] L. V. Keldysh, Soviet Journal of Experimental and Theoretical Physics Letters **29**, 658 (1979).
[21] A. Molina-Sánchez, K. Hummer, and L. Wirtz, Surface Science Reports **70**, 554 (2015).
[22] J. Hong, R. Senga, T. Pichler, and K. Suenaga, Phys. Rev. Lett. **124**, 087401 (2020).
[23] P. Cudazzo, L. Sponza, C. Giorgetti, L. Reining, F. Sottile, and M. Gatti, Phys. Rev. Lett. **116**, 066803 (2016).
[24] E. Malic, M. Selig, M. Feierabend, S. Brem, D. Christiansen, F. Wendler, A. Knorr, and G. Berghäuser, Phys. Rev. Materials **2**, 014002 (2018).
[25] X.-X. Zhang, T. Cao, Z. Lu, Y.-C. Lin, F. Zhang, Y. Wang, Z. Li, J. C. Hone, J. A. Robinson, D. Smirnov, S. G. Louie, and T. F. Heinz, Nature Nanotechnology **12**, 883 (2017).
[26] M. R. Molas, C. Faugeras, A. O. Slobodeniuk, K. Nogajewski, M. Bartos, D. M. Basko, and M. Potemski, 2D Materials **4**, 021003 (2017).
[27] H. C. Nerl, K. T. Winther, F. S. Hage, K. S. Thygesen, L. Houben, C. Backes, J. N. Coleman, Q. M. Ramasse, and V. Nicolosi, npj 2D Materials and Applications **1**, 2 (2017).
[28] F. Wu, F. Qu, and A. H. MacDonald, Phys. Rev. B **91**, 075310 (2015).
[29] D. Y. Qiu, T. Cao, and S. G. Louie, Phys. Rev. Lett. **115**, 176801 (2015).
[30] D. Y. Qiu, F. H. da Jornada, and S. G. Louie, Phys. Rev. B **93**, 235435 (2016).
[31] T. Deilmann and K. S. Thygesen, 2D Materials **6**, 035003 (2019).
[32] H. Yu, M. Laurien, Z. Hu, and O. Rubel, Phys. Rev. B **100**, 125413 (2019).
[33] P.-Y. Lo, G.-H. Peng, W.-H. Li, Y. Yang, and S.-J. Cheng, "Symmetry governed valley-pseudospin textures of the full-zone excitonic bands of transition-metal dichalcogenide monolayers," (2020), arXiv:2009.13183 [cond-mat.mes-hall].
[34] T. Galvani, F. Paleari, H. Miranda, A. Molina-Sánchez, L. Wirtz, S. Latil, H. Amara, and F. Ducastelle, ArXiv e-prints (2016), arXiv:1605.09581 [cond-mat.mtrl-sci].
[35] D. Gunlycke and F. Tseng, Phys. Chem. Chem. Phys. **18**, 8579 (2016).
[36] J. Koskelo, G. Fugallo, M. Hakala, M. Gatti, F. Sottile, and P. Cudazzo, Phys. Rev. B **95**, 035125 (2017).
[37] G. Strinati, Rivista del Nuovo Cimento **11**, 1 (1988).
[38] W. Hanke and L. J. Sham, Phys. Rev. Lett. **43**, 387 (1979).
[39] G. Onida, L. Reining, and A. Rubio, Rev. Mod. Phys. **74**, 601 (2002).
[40] R. M. Martin, L. Reining, and D. M. Ceperley, *Interacting Electrons: Theory and Computational Approaches* (Cambridge University Press, 2016).
[41] L. Hedin, Phys. Rev. **139**, A796 (1965).
[42] P. Cudazzo, M. Gatti, and A. Rubio, Phys. Rev. B **86**, 195307 (2012).
[43] B. Arnaud, S. Lebègue, P. Rabiller, and M. Alouani, Phys. Rev. Lett. **96**, 026402 (2006).
[44] A. Molina-Sánchez, D. Sangalli, K. Hummer, A. Marini, and L. Wirtz, Phys. Rev. B **88**, 045412 (2013).
[45] W. Kohn and L. J. Sham, Phys. Rev. **140**, A1133 (1965).
[46] N. Troullier and J. L. Martins, Phys. Rev. B **43**, 1993 (1991).
[47] R. G. Dickinson and L. Pauling, Journal of the American Chemical Society **45**, 1466 (1923), http://dx.doi.org/10.1021/ja01659a020.
[48] A. Ramasubramaniam, Phys. Rev. B **86**, 115409 (2012).
[49] D. Y. Qiu, F. H. da Jornada, and S. G. Louie, Phys. Rev. Lett. **111**, 216805 (2013).
[50] T. Cheiwchanchamnangij and W. R. L. Lambrecht, Phys. Rev. B **85**, 205302 (2012).
[51] K. F. Mak, C. Lee, J. Hone, J. Shan, and T. F. Heinz, Phys. Rev. Lett. **105**, 136805 (2010).
[52] I. Tamm, J. Phys. (USSR) **9**, 449 (1945).
[53] S. M. Dancoff, Phys. Rev. **78**, 382 (1950).
[54] S. Ismail-Beigi, Phys. Rev. B **73**, 233103 (2006).
[55] C. A. Rozzi, D. Varsano, A. Marini, E. K. U. Gross, and A. Rubio, Phys. Rev. B **73**, 205119 (2006).
[56] X. Gonze, G. M. Rignanese, M. Verstraete, J. M. Beuken, Y. Pouillon, R. Caracas, F. Jollet, M. Torrent, G. Zerah, M. Mikami, P. Ghosez, M. Veithen, J. Y. Raty, V. Olevano, F. Bruneval, L. Reining, R. Godby, G. Onida, D. R. Hamann, and D. C. Allan, Z. Kristallogr. **220**, 558 (2005).

[57] See http://www.bethe-salpeter.org.
[58] A. Chernikov, T. C. Berkelbach, H. M. Hill, A. Rigosi, Y. Li, O. B. Aslan, D. R. Reichman, M. S. Hybertsen, and T. F. Heinz, Phys. Rev. Lett. **113**, 076802 (2014).
[59] B. Zhu, X. Chen, and X. Cui, Scientific Reports **5**, 9218 EP (2015), article.
[60] P. Cudazzo, F. Sottile, A. Rubio, and M. Gatti, Journal of Physics: Condensed Matter **27**, 113204 (2015).
[61] C. Habenicht, M. Knupfer, and B. Büchner, Phys. Rev. B **91**, 245203 (2015).
[62] A. Marini, Phys. Rev. Lett. **101**, 106405 (2008).
[63] G. Fugallo, M. Aramini, J. Koskelo, K. Watanabe, T. Taniguchi, M. Hakala, S. Huotari, M. Gatti, and F. Sottile, Phys. Rev. B **92**, 165122 (2015).
[64] K. F. Mak, C. Lee, J. Hone, J. Shan, and T. F. Heinz, Phys. Rev. Lett. **105**, 136805 (2010).
[65] A. Splendiani, L. Sun, Y. Zhang, T. Li, J. Kim, C.-Y. Chim, G. Galli, and F. Wang, Nano Letters **10**, 1271 (2010), pMID: 20229981, http://dx.doi.org/10.1021/nl903868w.
[66] A. Stacy and D. Hodul, Journal of Physics and Chemistry of Solids **46**, 405 (1985).
[67] S. Galambosi, L. Wirtz, J. A. Soininen, J. Serrano, A. Marini, K. Watanabe, T. Taniguchi, S. Huotari, A. Rubio, and K. Hämäläinen, Phys. Rev. B **83**, 081413 (2011).